AUTONOMOUS ATTITUDE ESTIMATION VIA STAR SENSING AND PATTERN RECOGNITION

J. L. Junkins and T. E. Strikwerda

Engineering Science and Mechanics
Virginia Polytechnic Institute and State University

ABSTRACT

We report results to date on the development of an autonomous, on board, near real time spacecraft attitude estimation technique. The approach will use CCD based star sensors to digitize relative star positions. Three microcomputers are envisioned, configured in parallel, to (i) determine star image centroids and delete spurious images, (ii) identify measured stars with stars in an on board catalog and determine discrete attitude estimates, (iii) integrate gyro rate measurements and determine optimal real time attitude estimates for use in the control system and for feedback to the star identification algorithm.

We present improved algorithms for the star identification. The discrete attitude estimation algorithm recovers thermally varying interlock angles between two star sensors. The optimal state estimation process recovers rate gyro biases in addition to real time attitude estimates.

Discussion of Slide Material

Figure 1.

For this technique, two star sensors are fixed to the spacecraft and to each other with interlock angles of, say, 60°-90°. Both fields of view (FOV) are sampled at the same instant in time and the star data are used to determine the vehicle attitude. We note that each field can be used independently to yield attitude but if both fields of view are functioning, the data are combined to yield an orientation with higher precision and to recover interlock angles as well. We expect to attain a pointing accuracy of at least $\leq$ 10 arc-sec. and probably $\leq$ 5 arc-sec.

Figure 2.

This figure shows schematically the parallel processing nature of this technique. Process A will cycle independently of Processes B and C since it will likely be the most rapid. Process B will obtain image coordinates from Process A at the beginning of each cycle and at the same time obtain estimated orientation angles from the Runge-Kutta integrator section of Process C. The run time of Process B will probably be the longest of the three but will also be quite variable. The output of Process B consists of three orientation angles and the covariance matrix obtained from the least-squares correction. These are used by Process C along with the estimated angles. We propose a Kalman filter algorithm to determine the optimal state estimate at the time associated with the current data from Process A. Process C will also update the estimated rate gyro biases. These are then used for the next Runge-Kutta integration. Process C will likely have a relatively fixed time budget.

Figure 3.

Figure 3 displays a summary of functions performed by Process A. CCD integration time is typically 0.1 - 1.0 sec. and readout time is < 0.1 sec. The primary function of Process A is to determine image centroids. Star images are defocused slightly to spread images over 3 x 3 or 4 x 4 pixels. The response of each pixel is used to interpolate positions to an accuracy of, say, one-tenth of a pixel.

A second important function is to detect and delete spurious images. Images which are moving relative to other stars will be deleted. Since the cycle time should be quite short we can track images over several frames before Process B requests new data.

The output of Process A will consist of image coordinates and brightness at the latest epoch, for all stars with intensity above some threshold. Each FOV is treated separately and passed to Process B.

Figure 4.

Process B is the most challenging process. Input data consist of image coordinates from each FOV and estimated attitude angles for the time associated with the image measurements. An on-board star catalog is accessed to yield coordinates for all catalog stars within some uncertainty border around the estimated FOV. These are sorted according to angle from the estimated boresight of the star sensor.

Angles between measured stars are compared with angles between catalog stars until a tentative match occurs. The three orientation angles are adjusted to bring computed image coordinates of catalog stars into agreement (in a least-squares sense) with the image coordinates from the FOV. We next test for additional star matches and repeat the adjustment.

The above steps are performed for both FOVs. If both sensors are functioning, the data are then combined to refine the attitude angles and the three interlock angles between FOV1 and FOV2.

Output of Process B is three orientation angles at the time associated with the image measurements.

Figure 5.

The image placement on a CCD star sensor is a function of six parameters: spacecraft orientation angles (ϕ,θ,ψ), star coordinates (α, δ), and the sensor focal length, f. The colinearity equations of Figure 5 express this relationship for (x,y) placement.

To simplify the computation we chose to store direction cosines for the star coordinates rather than (α,δ). Note that once [C] is computed for an estimated orientation, image coordinates are simple algebraic equations.

Figure 6.

In process B, the cosines of interstar angles are computed and compared. Computation involves only algebraic expressions containing no trignometric functions. The star catalog contains direction cosines for each star rather than right ascension and declination (α,δ). Although more memory is required by the catalog, the speed gain by eliminating many sine and cosine calculations justifies the storage of direction cosines.

Figure 7.

Once a tentative star pair cosine from the catalog matches a measured pair cosine, the estimated orientation is iteratively adjusted

by least-squares differential correction. This scheme is used for both fields and the combined solution. In the latter case, three interlock angles are solved for as well as the three orientation angles.

Figure 8.

Figure 8 displays the stars accessed from the catalog for a typical case. The dashed line is the estimated FOV and the solid line represents the true FOV. The boxed stars are the stars that provided the first match with the measured stars.

The sky has been divided into 256 non-overlapping cells, all nearly the same size. One or more cells are accessed for stars near the bore-sight. Only those stars that are within an uncertainty border (~11°) are used in the pairing logic. In this example, three cells were accessed giving 73 stars of which 38 were used in pairing logic. A match was found on the 38th attempt and, after correction, all four measured stars were matched with catalog stars.

Only one cell, containing 24 stars, was needed for FOV2. A match was found on the fourth attempt and 1 additional star of the 5 measured stars was identified in the catalog after correction. The remaining 2 measured stars were not contained in the catalog.

Table 1.

In this table we list the angle corrections obtained by a typical least-squares solution in Process B. The three attitude angles have been perturbed by approximately three degrees and the interlock angles by 1 arc-minute.

As can be seen from the table, most of the attitude corrections are obtained by the FOV1 solution. The attitude is corrected again by the FOV2 solution due to poor interlock angles. Finally, the combined solution recovers both the attitude and interlock angles.

Figure 9.

Figure 9 presents an outline of the main function of Process C. The actual algorithms to be used have not been finalized pending evaluation of Process B execution time in a microcomputer system. Short run times for Process B will allow less complexity in Process C algorithms.

Presently, there are two primary tasks for Process C:

1) Integrate the equations of motion ahead to the time of Process A output to B. This will use the last output of Process C for the initial attitude state and gyro rates will have biases subtracted.

2) Use Extended Kalman Filter formulation to obtain the optimal best estimate of the spacecraft attitude at the instant of Process A output. Optimal estimates of gyro biases are also calculated. This algorithm requires the estimated angles from 1) above, the discrete attitude and associated covariance matrix obtained from the Process B solution, and the state covariance matrix from the last Kalman filter update. The best estimates of angles and biases are then used for subsequent integration of the motion equations.

Figure 10.

This figure demonstrates the behavior of the Kalman filter on simulated data. The plotted data show the deviations of the first attitude angle (ϕ) from the true orientation. Attitude from Process B is simulated by perturbing the true orientation angles (standard deviation of 8.8 arc-sec). The gyro rates are perturbed from a constant value ($\sim 4 \times 10^{-4}$ rad./sec.; standard deviation of 1.5×10^{-6} rad./sec.) each time they are needed and biases are set to 4.8×10^{-6} rad./sec. The initial estimated state is off

10° in each angle from the truth (very conservative) and biases are set to zero.

The attitude state is integrated ahead in 1 minute intervals and the deviation from the truth calculated (shown as "X"). Simulated data from Process B then becomes available and the Kalman filter applied. The deviations of the filtered results from the truth is denoted by crosses ("+"). Due to noisy gyro rate data and the 1 minute integration time, the filtered attitude nearly equals the Process B attitude.

The dashes ("-") are the estimated deviations as calculated from the updated covariance matrix after each pass through the Kalman filter.

Note that after only three Kalman filter applications the attitude and biases have been recovered, and the steady state attitude errors are less than 10 arc-seconds in all cases and usually less than 5 arc-seconds. The one minute interval between star-determined orientation estimates (from Process B) will in practice be variable and typically less than one minute; the precision of these simulated converged estimates is therefore felt to be conservative.

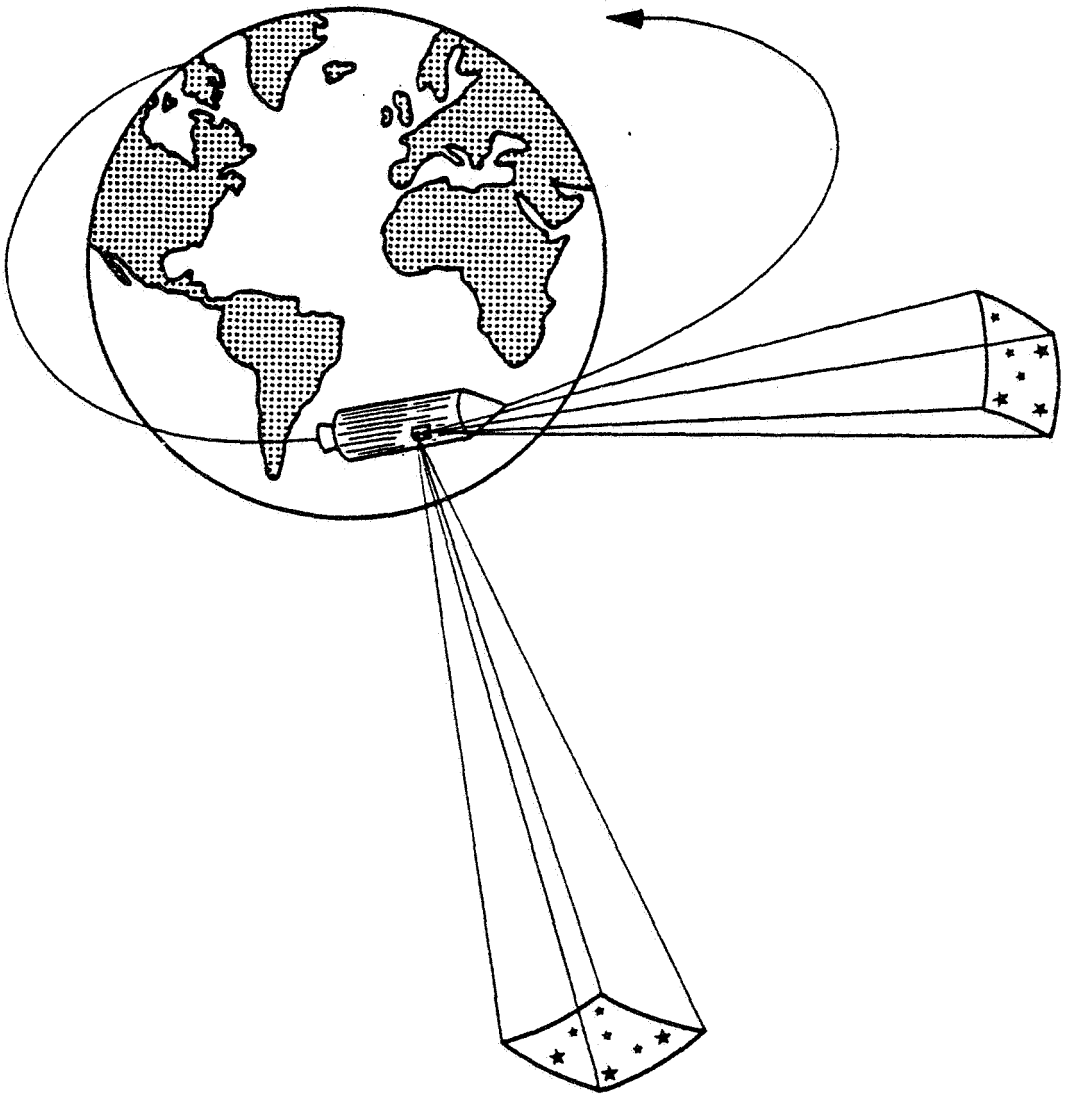

FIGURE 1 UVASTAR An electro-optical/software system capable of real time readout of digitized star coordinates, and ultimately, autonomous, near-real time star pattern recognition and attitude determination.

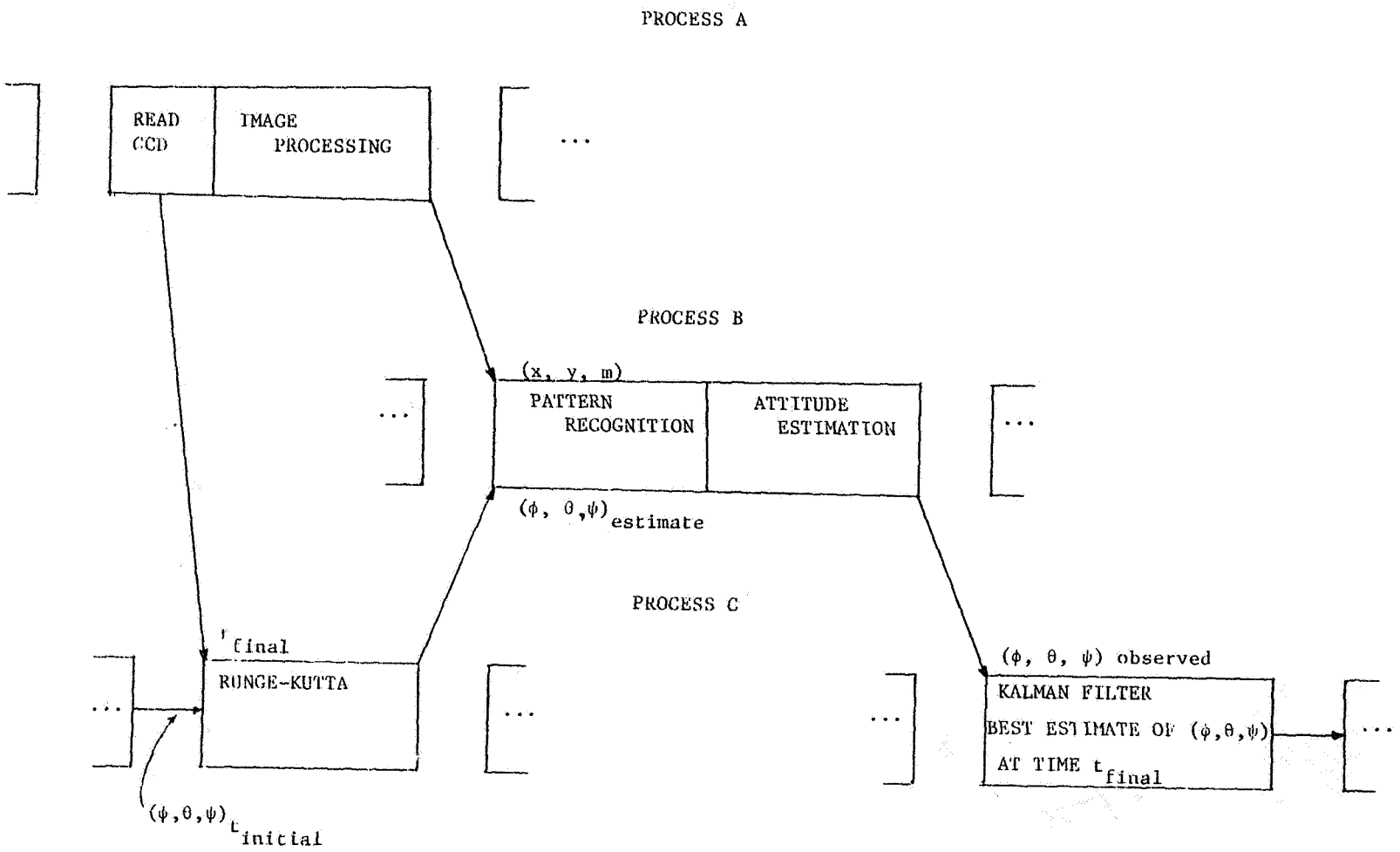

Figure 2: Three parallel process technique of star pattern recognition/attitude determination. Time runs from left to right.

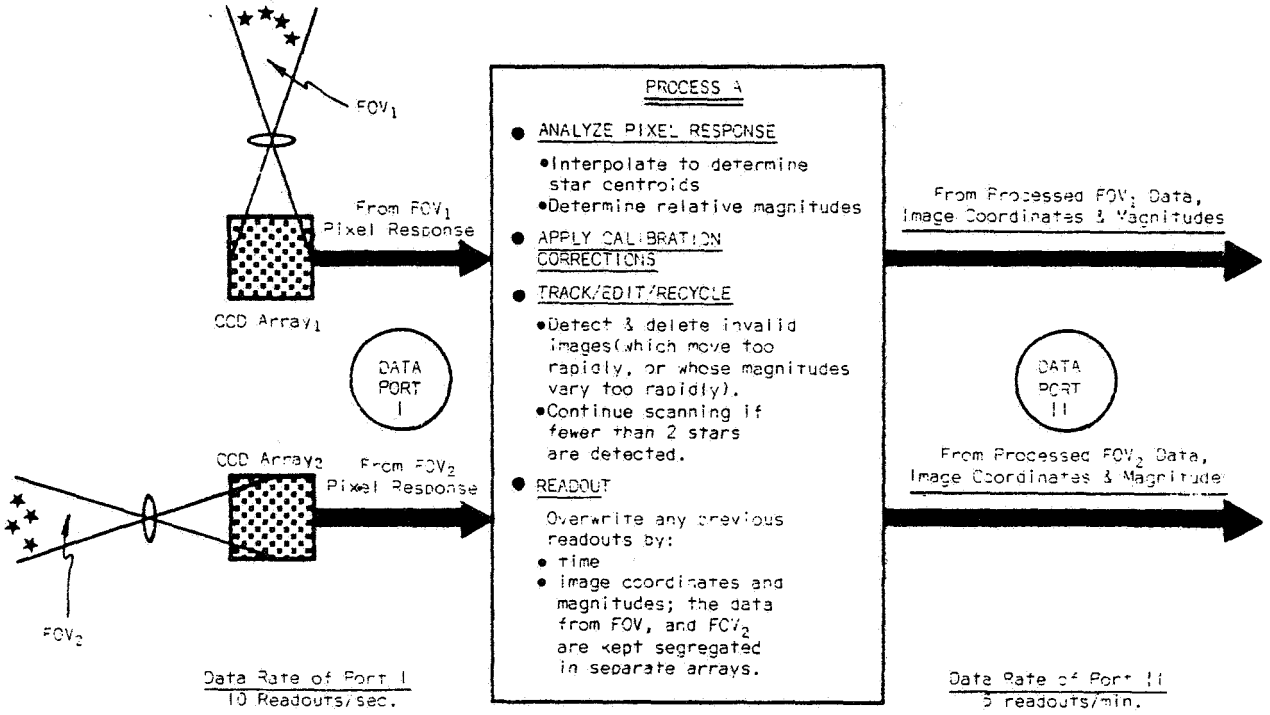

Figure 3: Major tasks of Process A.

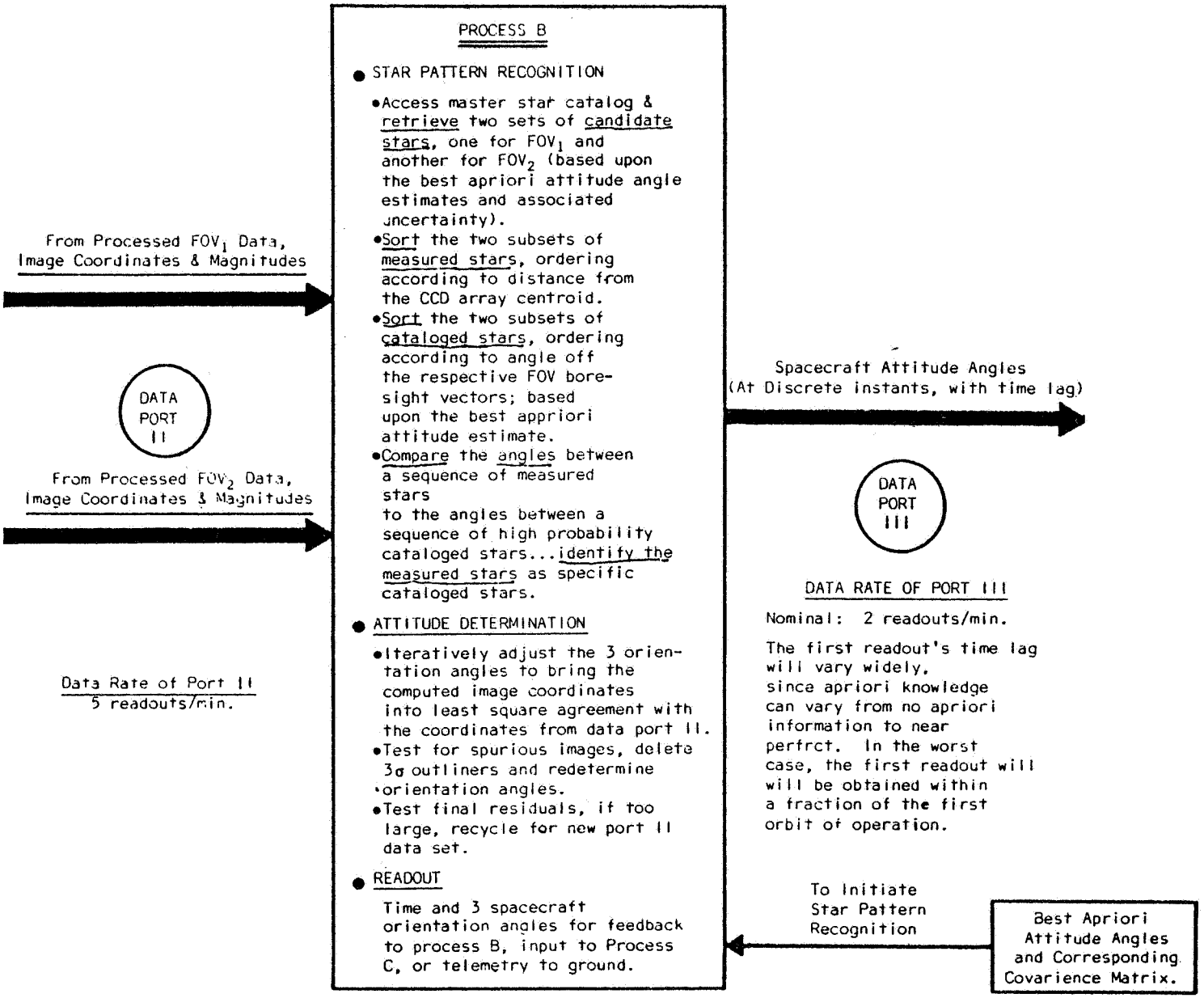

Figure 4: Major tasks of Process B.

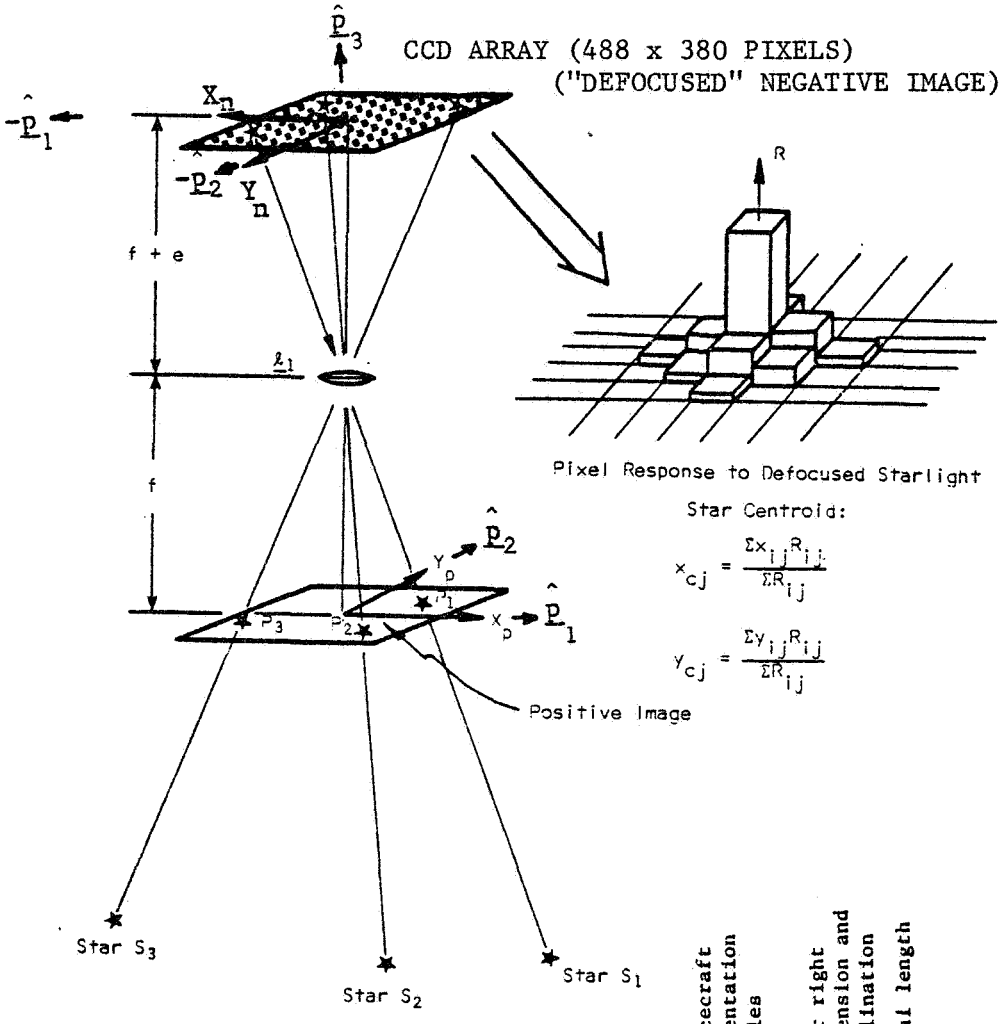

Colinearity Equations:

$$X_n = f\left[\frac{C_{11}L_1 + C_{12}L_2 + C_{13}L_3}{C_{31}L_1 + C_{32}L_2 + C_{33}L_3}\right] = \text{function}\ (\underbrace{\phi, \theta, \psi}_{\text{Spacecraft Orientation Angles}}, \underbrace{\alpha, \delta}_{\text{Star right Ascension and Declination}}, \underbrace{f}_{\text{Focal length}})$$

$$Y_n = f\left[\frac{C_{21}L_1 + C_{22}L_2 + C_{23}L_3}{C_{31}L_1 + C_{32}L_2 + C_{33}L_3}\right] = \text{function}\ (\phi, \theta, \psi, \alpha, \delta, f)$$

where

$$\left.\begin{aligned} L_1 &= \cos\delta\cos\alpha \\ L_2 &= \cos\delta\sin\alpha \\ L_3 &= \sin\delta \end{aligned}\right\} \text{ star direction cosines, } [C_{ij}] = \begin{bmatrix} \cos\psi & \sin\psi & 0 \\ -\sin\psi & \cos\psi & 0 \\ 0 & 0 & 1 \end{bmatrix} \begin{bmatrix} \cos\theta & 0 & -\sin\theta \\ 0 & 1 & 0 \\ \sin\theta & 0 & \cos\theta \end{bmatrix} \begin{bmatrix} 1 & 0 & 0 \\ 0 & \cos\phi & \sin\phi \\ 0 & -\sin\phi & \cos\phi \end{bmatrix}$$

FIGURE 5: Formation of Image on the CCD Array.

STAR PAIR COSINE CALCULATION

Measured Star Pair Cosine

$$\cos\theta_{mij} = \frac{\underline{\ell}_i \cdot \underline{\ell}_i}{|\underline{\ell}_i| \cdot |\underline{\ell}_j|}$$

$$= \frac{x'_i x'_j + y'_i y'_j + 1}{\sqrt{x'^2_i + y'^2_i + 1} \cdot \sqrt{x'^2_j + y'^2_j + 1}}$$

where $x' = x/f.l.$

$y' = y/f.l.$

(x,y) output of Process A

Cataloged Star Pair Cosine

$$\cos\theta_{cIJ} = \underline{L}_I \cdot \underline{L}_J$$

where $\underline{L}_I$ = unit vector towards I^{th} star in

catalog subset = $\begin{Bmatrix} L_{x_I} \\ L_{y_I} \\ L_{z_I} \end{Bmatrix} = \begin{Bmatrix} \cos\alpha_I \cos\delta_I \\ \sin\alpha_I \cos\delta_I \\ \sin\delta_I \end{Bmatrix}$

$\underline{L}_J$ = unit vector towards J^{th} star in catalog subset

(α,δ) = catalog right ascension and declination of stars from catalog.

Figure 6: Star pair cosine calculations for measured star pairs and catalog star pairs. f.l. is the star sensor focal length.

$$\begin{Bmatrix} \phi \\ \theta \\ \psi \end{Bmatrix}^{(k+1)} = \begin{Bmatrix} \phi \\ \theta \\ \psi \end{Bmatrix}^{(k)} + [(A^T A)^{-1} A^T]^{(k)} \begin{Bmatrix} x_i - x_i^{(k)} \\ y_i - y_i^{(k)} \\ x_j - x_j^{(k)} \\ y_j - y_j^{(k)} \end{Bmatrix}$$

where $A^{(k)} =$

$$\begin{bmatrix} \frac{\partial x_i^{(k)}}{\partial \phi^{(k)}} & \frac{\partial x_i^{(k)}}{\partial \theta^{(k)}} & \frac{\partial x_i^{(k)}}{\partial \psi^{(k)}} \\ \frac{\partial y_i^{(k)}}{\partial \phi^{(k)}} & \frac{\partial y_i^{(k)}}{\partial \theta^{(k)}} & \frac{\partial y_i^{(k)}}{\partial \psi^{(k)}} \\ \frac{\partial x_j^{(k)}}{\partial \phi^{(k)}} & \frac{\partial x_j^{(k)}}{\partial \theta^{(k)}} & \frac{\partial x_j^{(k)}}{\partial \psi^{(k)}} \\ \frac{\partial y_j^{(k)}}{\partial \phi^{(k)}} & \frac{\partial y_j^{(k)}}{\partial \theta^{(k)}} & \frac{\partial y_j^{(k)}}{\partial \psi^{(k)}} \end{bmatrix}$$

Figure 7: Method of least squares for estimated attitude angle correction. (ϕ,θ,ψ) are orientation angles and (x,y) are image coordinates.

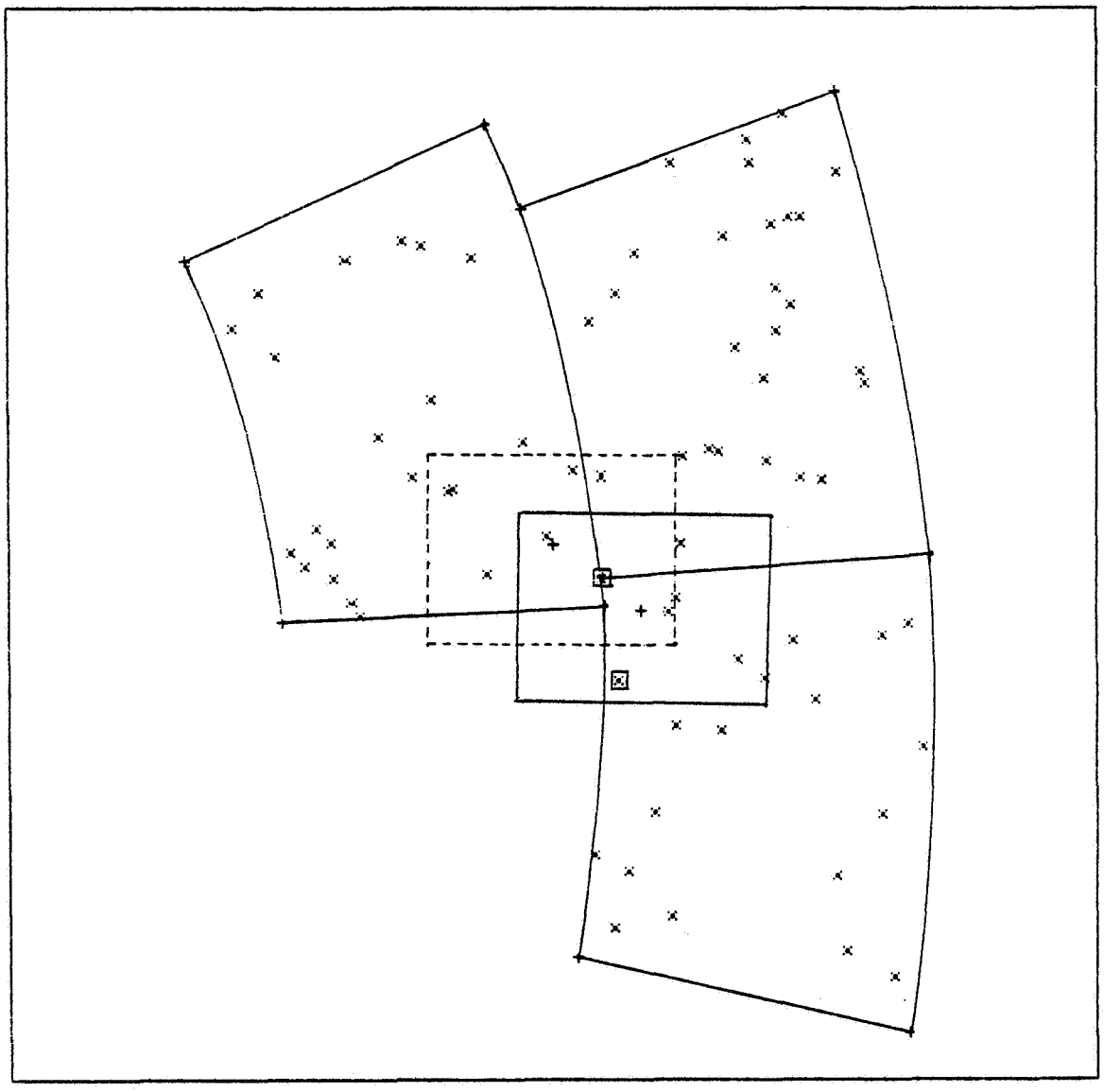

Figure 8: Boundaries of the true field of view (solid rectangle) and estimated field of view (dashed rectangle). Center of each FOV is denoted by "+". The three large sectors are the three cells accessed by Process B. The pair of boxed stars is the first pair to match the measured stars. FOV is approximately 7° x 9°.

TABLE 1: Iterative Least Square Attitude Determination

	Iteration	Orientation Angles (rad.) ϕ	θ	ψ	Interlock Angles (rad.) γ_1	γ_2	γ_3	Residual RSM (mm)	No. of Stars
FOV1	0	2.46254	0.03454	1.42654	—	—	—	3.550	2
	1	2.41509	0.08674	1.47404	—	—	—	0.166	2
	2	2.41254	0.08474	1.47688	—	—	—	0.011	2
	3	2.41254	0.08453	1.47689	—	—	—	0.001	2
	4	2.41253	0.08453	1.47672	—	—	—	0.002	4
FOV2	0	2.41253	0.08453	1.47672	1.57051	-1.57051	-1.57109	0.019	2
	1	2.41275	0.08289	1.47674	—	—	—	0.000	2
	3	2.41277	0.08345	1.47678	—	—	—	0.002	3
COMBINED (FOV1 + FOV2)	0	2.41277	0.08345	1.47678	1.57051	-1.57051	-1.57109	0.042	7
	1	2.41253	0.08453	1.47672	1.57059	-1.57085	-1.57003	0.002	7
	True	2.41254	0.08454	1.47654	1.57080	-1.57080	-1.57080	0.0034	

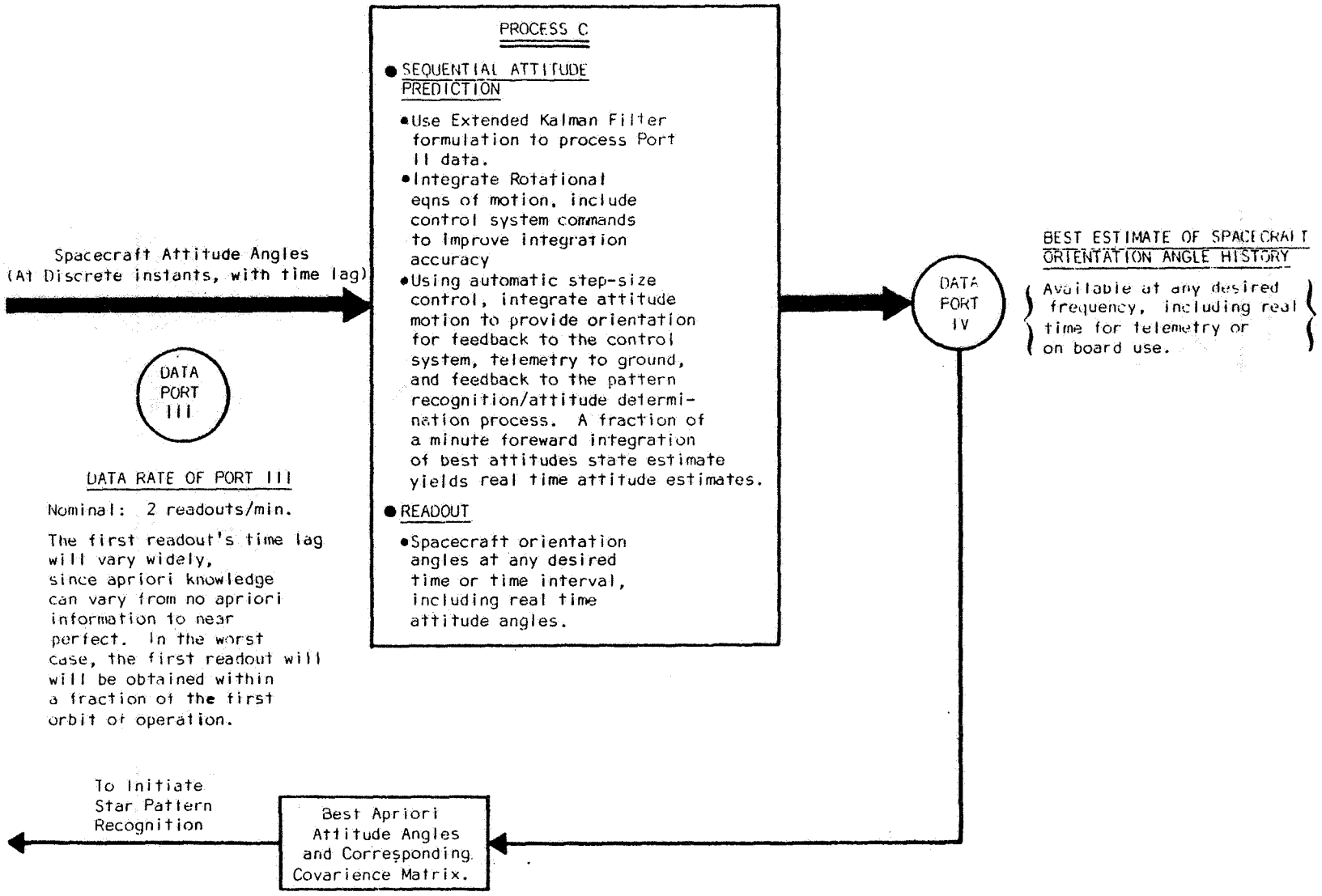

Figure 9: Major tasks of Process C.

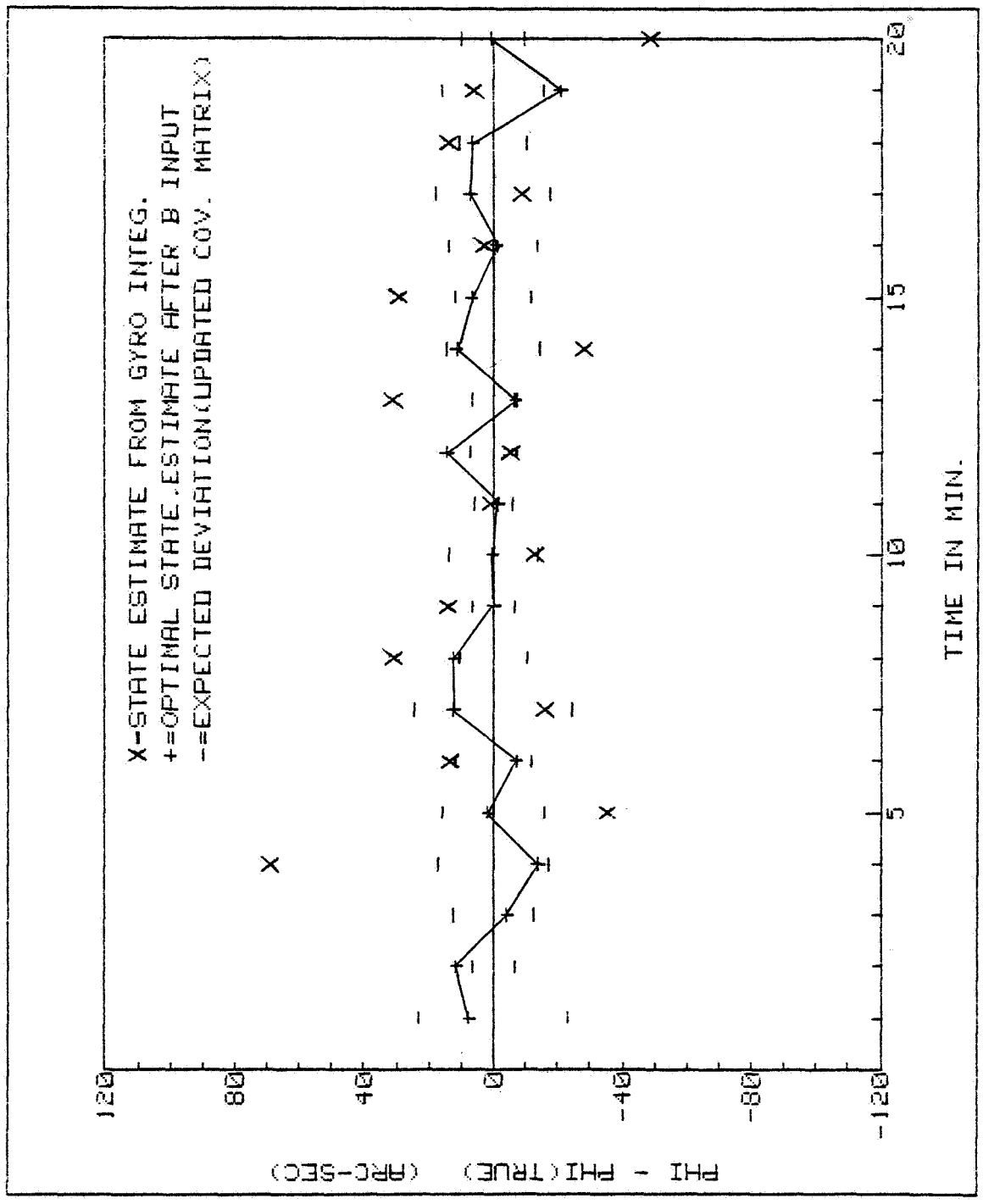

Figure 10: Behavior of Kalman filter for first

Figure 11: Concluding Remarks

- A new spacecraft attitude estimation approach is under development. Key features are:

  *Electro-optical star sensors with no moving parts

  *On board, near real time attitude estimation

  *Sub ten arc-second precision appears feasible.

- A three parallel process division of labor is proposed:

  A - Star-sensing/Image processing

  B - Star identification/Discrete attitude estimation

  C - Motion integration/Attitude estimation

- The software for Processes B and C is currently being implemented on microcomputers. The algorithms will be tested, evaluated and modified to maximize data throughput and accuracy.

- Area of major effort and/or problems:

  *Limited precision and speed obtained with on-board microcomputers

  *Data acquisition rate vs. Process B run time

  *Process B run time vs. Process C complexity.

References

Junkins, J. L., White, C. C., and Turner, J. D., "Star Pattern Recognition/ Attitude Determination using Digital Star Sensing," Proceedings of the Flight Mechanics/Estimation Theory Symposium (Goddard Space Flight Center, Greenbelt, Maryland, October, 1976).

Junkins, J. L., White, C. C., and Turner, J. D., "Star Pattern Recognition for Real Time Attitude Determination," Journal of the Astronautical Sciences, Vol. XXV, No. 3, July-Sept. 1977, 251-270.